

## Nanoparticle-Mediated Intervalence Transfer

Wei Chen,<sup>†</sup> Shaowei Chen,<sup>\*,†</sup> Feizhi Ding,<sup>‡</sup> Haobin Wang,<sup>\*,‡</sup> Lauren E. Brown,<sup>†</sup> and Joseph P. Konopelski<sup>†</sup>

Department of Chemistry and Biochemistry, University of California, Santa Cruz, California 95064 and Department of Chemistry and Biochemistry, New Mexico State University, Las Cruces, New Mexico 88003

Received May 23, 2008; E-mail: schen@chemistry.ucsc.edu; Haobin@nmsu.edu

**Abstract:** Nanoparticle-mediated intervalence transfer was reported with ferrocene moieties that were attached onto the ruthenium nanoparticle surface by ruthenium–carbene  $\pi$  bonds. The resulting particles exhibited two pairs of voltammetric waves with a potential spacing of about 200 mV and a rather intense absorption peak in the near-infrared range ( $\sim 1930$  nm) at mixed valence. Both features suggested Class II characteristics of the intraparticle intervalence transfer that mainly arose from through-bond interactions between the metal centers. Quantum calculations based on density functional theory showed that the nanoparticle core electrons served as conducting band states for the effective charge delocalization between particle-bound ferrocene moieties.

## Introduction

Monolayer-protected transition-metal nanoparticles represent a family of nanocomposite materials that exhibit unique electron-transfer characteristics. Most of these particles are stabilized by mercapto derivatives.<sup>1,2</sup> Yet because of the lack of interesting chemistry of the metal–thiolate linkage, the impact of the metal–ligand interfacial contacts on the nanoparticle charge-transfer chemistry has been largely ignored. In contrast, when nanoparticles are passivated by metal–carbon covalent bonds, new optoelectronic properties emerge.<sup>3–7</sup> Recently, ruthenium nanoparticles stabilized by ruthenium–carbene covalent bonds have been prepared.<sup>6</sup> The resulting Ru=C  $\pi$  linkage may thus be exploited as a unique mechanism for ligand–core charge delocalization, leading to nanoparticle-mediated electronic communication between particle-bound functional moieties and consequently the emergence of new optoelectronic properties. Such an unprecedented degree of control of the particle materials properties is further powered by the olefin metathesis reactions of these carbene-stabilized nanoparticles with vinyl-terminated derivatives, where multiple and versatile functional moieties can be incorporated onto individual nanoparticles.<sup>6,7</sup>

Traditionally, electronic communication refers to intervalence charge transfer between two or more identical molecular

moieties at mixed valence that are linked by a conjugated molecular bridge<sup>8–13</sup> and has been typically observed in organometallic complexes.<sup>14</sup> Depending on the degree of charge delocalization or the extent of interactions ( $\alpha$ ) between the functional moieties, three classes of compounds have been identified by Robin and Day.<sup>15</sup> Class I refers to the compounds that exhibit little or no interaction ( $\alpha \approx 0$ ), whereas in Class III compounds extensive charge delocalization occurs ( $\alpha = 0.707$ ), and Class II compounds fall into the intermediate range ( $0 < \alpha < 0.707$ ). Quantum mechanically, delocalization from one metal center to another in a complex is primarily determined by two contributing factors: (i) direct overlap of the orbitals of the two metal centers (i.e., through-space interactions) and (ii) metal–ligand–metal overlap that may involve  $\sigma$  or  $\pi$  metal–ligand bonds (i.e., through-bond interactions). When the metal centers are separated by a sufficiently long distance, the contribution from the first factor will be minimal whereas the second contribution becomes predominant, which can be readily varied by the specific ligand structure and metal–ligand interactions. For instance, for biferrocene (a Class II compound)<sup>8</sup> intervalence charge transfer leads to the appearance of two voltammetric waves instead of one voltammetric wave corresponding to the

(8) Cowan, D. O.; Levanda, C.; Park, J.; Kaufman, F. *Acc. Chem. Res.* **1973**, *6*, 1–7.

(9) Day, P.; Hush, N. S.; Clark, R. J. H. *Philos. Trans. R. Soc., Ser. A: Math. Phys. Eng. Sci.* **2008**, *366*, 5–14.

(10) Gamelin, D. R.; Bominaar, E. L.; Mathoniere, C.; Kirk, M. L.; Wieghardt, K.; Girerd, J. J.; Solomon, E. I. *Inorg. Chem.* **1996**, *35*, 4323–4335.

(11) Williams, R. D.; Petrov, V. I.; Lu, H. P.; Hupp, J. T. *J. Phys. Chem. A* **1997**, *101*, 8070–8076.

(12) Brunschwigg, B. S.; Creutz, C.; Sutin, N. *Chem. Soc. Rev.* **2002**, *31*, 168–184.

(13) Sun, H.; Steeb, J.; Kaifer, A. E. *J. Am. Chem. Soc.* **2006**, *128*, 2820–2821.

(14) Concepcion, J. J.; Dattelbaum, D. M.; Meyer, T. J.; Rocha, R. C. *Philos. Trans. R. Soc., Ser. A: Math. Phys. Eng. Sci.* **2008**, *366*, 163–175.

(15) Robin, M. B.; Day, P. *Adv. Inorg. Chem. Radiochem.* **1967**, *10*, 247–422.

<sup>†</sup> University of California, Santa Cruz.

<sup>‡</sup> New Mexico State University.

(1) Brust, M.; Walker, M.; Bethell, D.; Schiffrin, D. J.; Whyman, R. *J. Chem. Soc., Chem. Commun.* **1994**, 801–802.

(2) Templeton, A. C.; Wuelfing, M. P.; Murray, R. W. *Acc. Chem. Res.* **2000**, *33*, 27–36.

(3) Mirkhalaf, F.; Paprotny, J.; Schiffrin, D. J. *J. Am. Chem. Soc.* **2006**, *128*, 7400–7401.

(4) Ghosh, D.; Chen, S. W. *J. Mater. Chem.* **2008**, *18*, 755–762.

(5) Ghosh, D.; Pradhan, S.; Chen, W.; Chen, S. W. *Chem. Mater.* **2008**, *20*, 1248–1250.

(6) Chen, W.; Davies, J. R.; Ghosh, D.; Tong, M. C.; Konopelski, J. P.; Chen, S. W. *Chem. Mater.* **2006**, *18*, 5253–5259.

(7) Tulevski, G. S.; Myers, M. B.; Hybertsen, M. S.; Steigerwald, M. L.; Nuckolls, C. *Science* **2005**, *309*, 591–594.

sequential redox reactions of the two iron centers, and in spectroscopic measurements a rather intense absorption peak is observed at mixed valence in the near-infrared (NIR) region (1800–1900 nm), which is ascribed to an intramolecular electron-transfer transition. These electrochemical and spectroscopic characteristics can be readily varied by the molecular structure of the chemical bridge that links the two ferrocene moieties. With a conjugated spacer, effective intervalence transfer can still occur; however, when bridged by  $sp^3$  carbons, the electronic communication diminishes drastically.<sup>16</sup>

It should be noted that so far these studies have been mostly confined to relatively simple organometallic molecular complexes, and none has involved nanoparticle molecules. Therefore, a fundamental question arises when redox-active moieties are bound onto a transition-metal nanoparticle surface through conjugated chemical bonds: will effective electronic communication take place between these particle-bound functional moieties? Four decades ago Hush<sup>17</sup> predicted that effective electron transfer between metal centers at the electrode/electrolyte interface might occur using extensively delocalized  $\pi$  systems as the chemical linkers. One would anticipate a similar response on the nanoscale particle surface. Yet, so far there has been no experimental validation of this prediction.

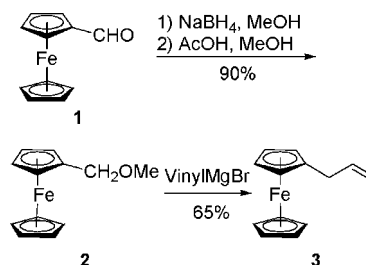
This is the primary motivation of the present study, where carbene-functionalized ruthenium nanoparticles are used as the nanoscale structural scaffold and ferrocene moieties are exploited as the molecular probe because of the well-known electrochemical and spectroscopic characteristics. Specifically, effective Class II intraparticle intervalence transfer is observed when the ferrocene moieties are bound onto the ruthenium nanoparticle surface by a conjugated linker (e.g., via olefin metathesis reaction with vinylferrocene), whereas control experiments with allylferrocene show that the presence of a  $sp^3$  carbon spacer results in Class I behavior.

## Experimental Section

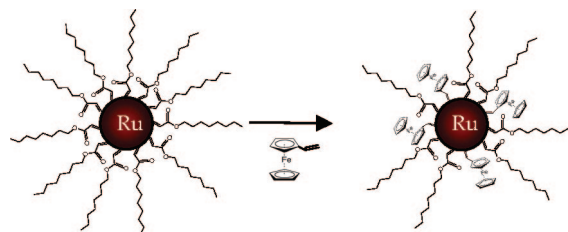
**Chemicals.** Ruthenium chloride ( $RuCl_3$ , 99+%, ACROS), 1,2-propanediol (ACROS), sodium acetate trihydrate ( $NaAc \cdot 3H_2O$ , MC&B), nitrosium hexafluorophosphate ( $NOPF_6$ , 95%, ACROS), tetrabutylammonium perchlorate (TBAP, 99%, ACROS), vinylferrocene (98%, ACROS), ferrocene carboxaldehyde (98%, Wind River Chemicals), and vinylmagnesium bromide (0.7 M solution in THF, ACROS) were used as received. Octyldiazoacetate was synthesized by following a modified literature procedure that was detailed previously.<sup>6,18</sup> All solvents were obtained from typical commercial sources and used without further treatment. Water was supplied by a Barnstead Nanopure water system ( $18.3 M\Omega \cdot cm$ ).

**Synthesis of Allylferrocene.** Synthesis of allylferrocene ( $CH_2=CH-CH_2-Fc$ ) is depicted in Scheme 1. First, methoxymethylferrocene **2** was synthesized from hydroxymethylferrocene (obtained by reduction of ferrocene carboxaldehyde) according to the literature procedure.<sup>19,20</sup> Then, methoxymethylferrocene **2** (5.3 g, 23 mmol) was placed in a one-necked round-bottom flask equipped with a Claisen distillation adapter and a reflux condenser under an atmosphere of nitrogen. Vinylmagnesium bromide (39 mL, 0.7 M in THF, 1.2 equiv) was added slowly, and the mixture was heated to 120 °C. After removal of the solvent by distillation,

Scheme 1



Scheme 2



the mixture was stirred at 120 °C for 4 h. The mixture was cooled to room temperature and dissolved in ether (200 mL). The resulting solution was washed with water (100 mL), dried over  $MgSO_4$ , and condensed to afford an orange oil. Flash column chromatography (10% methylene chloride in hexanes) gave allylferrocene (3.4 g, 65%).  $^1H$  NMR (500 MHz,  $CDCl_3$ ):  $\delta$  = 6.13 (m, 1H), 5.24–5.14 (m, 2H), 4.25 (s, 5H), 4.21–4.18 (m, 4H), 3.21 (dt,  $J$  = 1.5, 8.3, 2H).  $^{13}C$  NMR (125 MHz,  $CDCl_3$ ):  $\delta$  = 137.44, 115.21, 87.08, 68.68, 68.15, 67.46, 33.81. IR (thin film):  $\nu_{max}$  = 3091, 1637, 1430, 1412, 1105, 816  $cm^{-1}$ . HRMS for  $[M^+]$   $C_{13}H_{14}Fe$  calcd 226.04394, found 226.03402. The  $^1H$  and  $^{13}C$  NMR spectra obtained in  $C_6D_6$  were consistent with the literature values.<sup>21</sup>

**Ruthenium Nanoparticle.** Synthesis of the ruthenium nanoparticles was reported earlier.<sup>6,7</sup> Briefly, ruthenium colloids were produced by thermolytic reduction of ruthenium chloride in 1,2-propanediol.<sup>22</sup> The resulting colloid was then mixed with octyldiazoacetate in toluene, where the strong affinity of the diazo moieties to the ruthenium surface led to formation of  $Ru=C$  carbene bonds and concurrent release of nitrogen.<sup>6</sup> The resulting purified nanoparticles were denoted as  $Ru=C8$ , which exhibited a core diameter of  $2.12 \pm 0.72$  nm as determined by transmission electron microscopy (TEM) measurements.<sup>6</sup> The  $Ru=C8$  particles obtained above were then subject to ligand exchange reactions with vinylferrocene ( $Fc-CH=CH_2$ ) by olefin metathesis reactions on the Ru surface (Scheme 2).<sup>6</sup> The resulting particles are referred to as  $Ru=CH-Fc$ . The surface coverage of the ferrocene moieties (typically 5–20% replacement) was quantitatively assessed by proton nuclear magnetic resonance ( $^1H$  NMR) measurements and readily varied by the initial feed ratio between vinylferrocene and the  $Ru=C8$  particles. Experimentally the metal cores of the  $Ru=CH-Fc$  particles were dissolved by dilute potassium cyanide (KCN) before the NMR spectra of the remaining organic components were acquired. The assignments of the resulting NMR features were aided by mass spectrometric study. Metathesis reactions of the  $Ru=C8$  particles with allylferrocene were carried out and characterized in a similar fashion.

**Spectroscopy.** UV–vis spectroscopic studies were performed with an ATI Unicam UV4 spectrometer, and NIR spectra were acquired with an Ocean Optics NIR-512 spectrometer. In both

(16) Nishihara, H. *Bull. Chem. Soc. Jpn.* **2001**, *74*, 19–29.

(17) Hush, N. S. *Electrochim. Acta* **1968**, *13*, 1005–1023.

(18) Danheiser, R. L.; Miller, R. F.; Brisbois, R. G.; Park, S. Z. *J. Org. Chem.* **1990**, *55*, 1959–1964.

(19) Delacroix, O.; Andriamihaja, B.; Picart-Goetgheluck, S.; Brocard, J. *Tetrahedron* **2004**, *60*, 1549–1556.

(20) Combs, C. S.; Willis, T. C.; Giles, R. D.; Stephens, W. D. *J. Org. Chem.* **1971**, *36*, 2027–2029.

(21) Wedeking, K.; Mu, Z. C.; Kehr, G.; Sierra, J. C.; Lichtenfeld, C. M.; Grimme, S.; Erker, G.; Frohlich, R.; Chi, L. F.; Wang, W. C.; Zhong, D. Y.; Fuchs, H. *Chem. Eur. J.* **2006**, *12*, 1618–1628.

(22) Chakroune, N.; Viau, G.; Ammar, S.; Poul, L.; Veautier, D.; Chehimi, M. M.; Mangency, C.; Villain, F.; Fievet, F. *Langmuir* **2005**, *21*, 6788–6796.

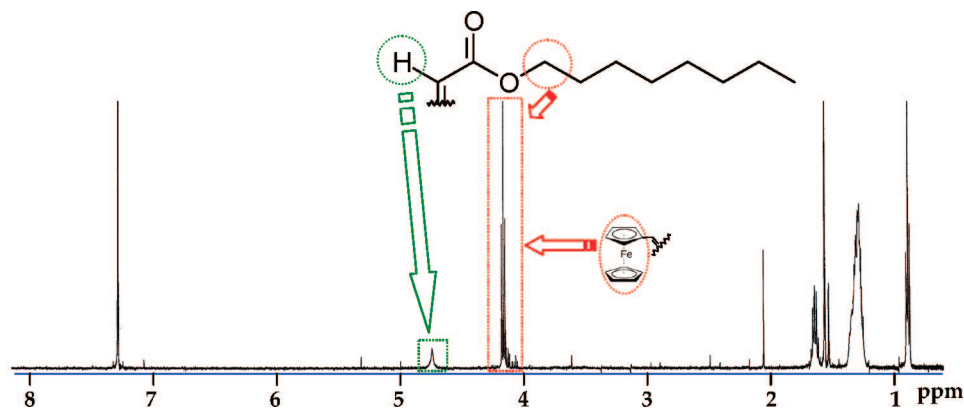


**Figure 1.** Representative  $^1\text{H}$  NMR spectrum (in  $\text{CDCl}_3$ ) of  $\text{Ru}=\text{CH}-\text{Fc}$  nanoparticles (sample III) after the metal cores were dissolved by diluted KCN.

measurements a 1-cm quartz cuvette was used.  $^1\text{H}$  NMR spectroscopic measurements were performed with a Varian Unity 500 MHz spectrometer. Low-resolution mass spectrometry was performed on a benchtop Mariner electrospray ionization time-of-flight instrument (ESITOF). Direct-inject and LC/MS analysis were performed on the organic extract following dissolution of the nanoparticles with aqueous potassium cyanide. Dichloromethane was removed by evaporation, and the crude residue was taken up in methanol for direct-inject analysis with positive-ion polarity. FTIR measurements were carried out with a Perkin-Elmer FTIR spectrometer (Spectrum One) where the samples were prepared by compressing the materials of interest into a KBr pellet. The spectral resolution was  $4\text{ cm}^{-1}$ .

**Electrochemistry.** Voltammetric measurements were carried out with a CHI 440 electrochemical workstation. A polycrystalline gold disk electrode (sealed in a glass tubing) was used as the working electrode. A Ag/AgCl wire and Pt coil were used as the (quasi)reference and counter electrodes, respectively. The gold electrode was first polished with alumina slurries of  $0.05\ \mu\text{m}$  and then cleansed by sonication in 0.1 M  $\text{HNO}_3$ ,  $\text{H}_2\text{SO}_4$ , and Nanopure water successively. Prior to data collection, the electrolyte solution was deaerated by bubbling ultra-high-purity  $\text{N}_2$  for at least 20 min and blanketed with a nitrogen atmosphere during the entire experimental procedure. Note that the electrode potentials were all calibrated against the formal potential of ferrocene monomers ( $\text{Fc}^+/\text{Fc}$ ) in the same solvent.

**Theoretical Calculations and Modeling.** The standard density functional theory (DFT) calculations were performed using the quantum chemical program Gaussian 03.<sup>23</sup> The B3LYP hybrid functional, which includes the Becke three-parameter exchange<sup>24</sup> and the Lee, Yang, and Parr correlation functionals,<sup>25</sup> was employed in all calculations. LANL2DZ basis sets<sup>26</sup> were used for metals Fe and Ru, whereas 6-31G\*\* basis sets<sup>27</sup> were assigned to C and H. Full geometric optimizations were performed for most of the systems except for the  $\text{Fc}-\text{CH}=(\text{Ru})_n-\text{CH}-\text{Fc}$  cluster system where only the two  $\text{Fc}-\text{CH}=\text{}$  groups were optimized while the Ru cluster was fixed to the bulk ruthenium structure. To obtain electronic coupling elements for various electron-transfer reactions the constrained DFT (CDFT) simulation was performed with the quantum chemical program NWChem<sup>28</sup> using the same basis functions as in the standard DFT study. In some calibration

calculations (Supporting Information) the solvent effect was taken into account by the COSMO method.<sup>29</sup>

## Results and Discussion

**Nanoparticle Preparation.** The structural details of the ruthenium nanoparticles were first characterized. Figure 1 depicts a representative  $^1\text{H}$  NMR spectrum of the  $\text{Ru}=\text{CH}-\text{Fc}$  nanoparticles after the metal core was dissolved by dilute KCN. The singlet peak at 4.74 ppm (green dashed box) was attributed to the methine proton of the carbene fragment,<sup>30</sup> and the peaks between 4.0 and 4.4 ppm (red dashed box) were ascribed to the combined contribution of the ferrocenyl ring protons and the  $\alpha$ -methylene protons of the carbene ligands.<sup>6</sup> The ratio between the integrated areas of these two peaks was then used to estimate the surface coverage of Fc on the particle surface, which is summarized in Table 1 as sample III. Nanoparticles with other ferrocene surface concentrations (5–20%) were prepared and characterized in a similar fashion, and the results are also included in Table 1.

Note that the above NMR peak assignments are aided largely by mass spectrometric measurements. Whereas the exact chemical structures of the organic extracts are somewhat unclear at the moment,<sup>31</sup> mass spectrometric measurements (Figure S1) did suggest formation of (i) heterodimers of the carbene and ferrocene fragments ( $m/z$  369.3), (ii) ketenimine derivatives of the carbene fragments ( $m/z$  199.1, likely as a result of the reaction of the carbene fragments with cyanide ions in solution), as well as (iii) derivatives of ferrocene ( $m/z$  186.1 and 211.9). Of these, both i and ii lead to the appearance of a singlet at 4.74 ppm for the methine proton in the NMR measurements (Figure 1) as well as a modestly intense band at  $2109\text{ cm}^{-1}$  in the FTIR measurements.<sup>30</sup> No polymeric products were detected in the mass spectrometric measurements.

(29) Klamt, A.; Schuurmann, G. *J. Chem. Soc., Perkin Trans. 2* **1993**, 799–805.

(30) Fulloon, B.; Elnabi, H. A. A.; Kollenz, G.; Wentrup, C. *Tetrahedron Lett.* **1995**, 36, 6547–6550.

(31) Note that this calculation provides a rough estimate as analysis was only possible on the compounds that were isolable following potassium cyanide treatment of the nanoparticles and assignments were made based on our limited knowledge of the identities of the compounds. Mechanistic studies on the nucleophilic attack on more electron-rich Fischer carbenes suggest that complete dissociation of the organic ligands from the metal under these conditions may be unlikely. See, for instance: Bernasconi, C. F. *Chem. Soc. Rev.* **1997**, 26, 299–307. Thus, efforts to more accurately quantify the exchange reactions are underway.

(23) Frisch, M. J., et al. Gaussian, Inc.: Wallingford, CT, 2004.

(24) Becke, A. D. *J. Chem. Phys.* **1993**, 98, 5648–5652.

(25) Lee, C. T.; Yang, W. T.; Parr, R. G. *Phys. Rev. B* **1988**, 37, 785–789.

(26) Hay, P. J.; Wadt, W. R. *J. Chem. Phys.* **1985**, 82, 270–283.

(27) Franchl, M. M.; Pietro, W. J.; Hehre, W. J.; Binkley, J. S.; Gordon, M. S.; Defrees, D. J.; Pople, J. A. *J. Chem. Phys.* **1982**, 77, 3654–3665.

(28) Bylaska, E. J., et al. Pacific Northwest National Laboratory: Richland, WA, 2006.

**Table 1.** Summary of Voltammetric Data of Ferrocene-Functionalized Ru Nanoparticles<sup>a</sup>

particles	Fc% <sup>b</sup>	$E_{p,c}$ (V)	$E_{p,a}$ (V)	$E^{\circ}$ (V)	$\Delta E_p$ (V)	$\Delta E^{\circ}$ (V)
Ru=CH-Fc (I)	5.9	-0.017	-0.013	-0.015	0.004	0.194
		0.177	0.181	0.179	0.004	
Ru=CH-Fc (II)	6.2	-0.014	-0.018	-0.016	0.004	0.180
		0.164	0.164	0.164	0	
Ru=CH-Fc (III)	10.5	-0.019	-0.019	-0.019	0	0.204
		0.177	0.193	0.185	0.016	
Ru=CH-Fc (IV)	12.9	-0.004	-0.007	-0.006	-0.003	0.219
		0.209	0.217	0.213	0.008	
Ru=CH-Fc (V)	13.5	-0.020	-0.014	-0.017	0.006	0.202
		0.180	0.190	0.185	0.010	
Ru=CH-Fc (VI)	21.3	0.027	0.013	0.020	0.014	0.217
		0.233	0.241	0.237	0.008	
Ru=CH-CH <sub>2</sub> -Fc	17.9	0.024	0.028	0.026	0.004	
		0.019	0.043	0.031	0.024	

<sup>a</sup> Data acquired from SWV measurements as exemplified in Figure 2.  $E_{p,c}$  denotes the cathodic peak potential,  $E_{p,a}$  the anodic peak potential,  $E^{\circ}$  the formal potential,  $\Delta E_p$  the peak splitting ( $=|E_{p,a} - E_{p,c}|$ ), and  $\Delta E^{\circ}$  the difference between the two formal potentials. <sup>b</sup> On the basis of <sup>1</sup>H NMR characterizations as exemplified in Figure 1.

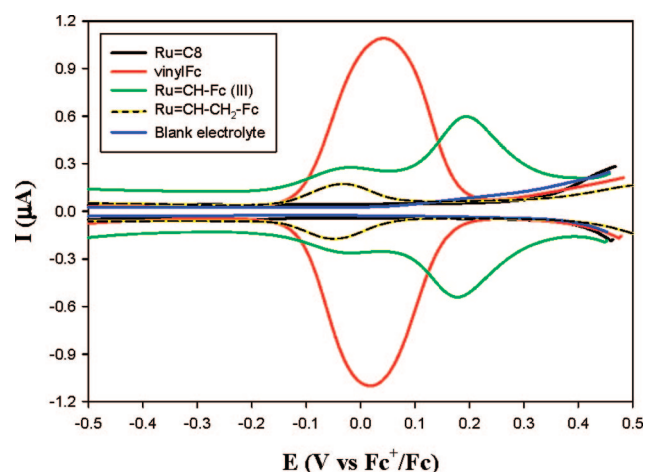


**Figure 2.** SWVs of vinylferrocene monomers (0.1 mM, red), Ru=C8 (4.7 mg/mL, black), Ru=CH-Fc (sample III, 5 mg/mL, green), and Ru=CH-CH<sub>2</sub>-Fc (2 mg/mL, yellow-black dashed) particles in DMF containing 0.1 M TBAP. Also shown is the SWV acquired after the electrode was removed from the Ru=CH-Fc particle solution, rinsed with DMF, and then immersed in a blank electrolyte (blue). Experimental conditions: Au disk electrode area 0.3 mm<sup>2</sup>, increment of potential 4 mV, amplitude 25 mV, and frequency 15 Hz.

Incorporation of the ferrocene moieties into the particle protecting layer was also confirmed by FTIR measurements. For instance, the ferrocene C-H vibrational bands at 1091 and 1462 cm<sup>-1</sup> were observed with both the Ru=CH-Fc nanoparticles and the vinylferrocene monomers. The vinyl (C=C) vibrational band observed at 1630 cm<sup>-1</sup> with the vinylferrocene monomers disappeared when the ligands underwent metathesis reaction and were bound to the Ru particle surface forming Ru=C  $\pi$  bonds.

Metathesis reactions of the Ru=C8 particles with allylferrocene (Fc-CH<sub>2</sub>-CH=CH<sub>2</sub>) were carried out in a similar fashion as a control experiment. <sup>1</sup>H NMR measurements showed that 17.9% of the protecting ligands of the resulting particles contained the ferrocene moieties (Table 1).

**Electrochemistry.** Voltammetric measurements of the ferrocene-functionalized ruthenium nanoparticles prepared above were then carried out. Figure 2 depicts the representative square wave voltammograms (SWVs) of vinylferrocene (vinylFc) monomers, Ru=C8, Ru=CH-Fc (sample III), and Ru=CH-CH<sub>2</sub>-Fc nanoparticles in dimethylformamide (DMF) containing 0.1 M tetrabutylammonium perchlorate (TBAP).

Interestingly, two pairs of voltammetric peaks can be seen with the Ru=CH-Fc particles (green curve) with the formal potentials ( $E^{\circ}$ ) at -0.019 and +0.185 V (vs Fc<sup>+</sup>/Fc), respectively (and hence a potential spacing of  $\Delta E^{\circ} = 0.204$  V). These voltammetric peaks are ascribed to the redox reaction of the ferrocene moieties, Fc<sup>+</sup> + e  $\leftrightarrow$  Fc, and the small peak splitting ( $\Delta E_p = 0$  and 16 mV) is consistent with the facile electron-transfer kinetics of the ferrocene moiety. The appearance of two pairs of voltammetric waves with the Ru=CH-Fc particles strongly suggests that intraparticle intervalence transfer occurs between the ferrocene centers through the ruthenium particle cores. Similar responses were observed for other Ru=CH-Fc particles in the series (Table 1). This is in sharp contrast to those of the Ru=C8 particles (black curve) that exhibit only featureless responses and to vinylferrocene monomers (red curve) which show only one pair of voltammetric peaks at +0.031 V within the same potential range.

Table 1 summarizes the voltammetric results of the six Ru=CH-Fc nanoparticles. Notably, it can be seen that the potential spacing ( $\Delta E^{\circ}$ ) is close to 0.20 V in DMF with the ferrocene surface coverage varied in the range of 5–20%. This is very comparable to those observed with biferrocene derivatives with a conjugated spacer,<sup>32,33</sup> suggestive of a Class II compound as defined by Robin and Day.<sup>15</sup> In fact, if we treat the Ru particle core as a conducting medium with fully delocalized electrons, the ferrocene moieties that are bound onto the Ru particle surface can be considered to be approximately equivalent to Fc-CH=CH-Fc.<sup>32</sup> Indeed, the  $\Delta E^{\circ}$  values are very comparable (0.20 V for Ru=CH-Fc and 0.17 V for Fc-CH=CH-Fc), where the small discrepancy may partly arise from the different solvent medium used as dictated by Marcus and Hush theory.<sup>34</sup> Note that the  $\Delta E^{\circ}$  value for biferrocene (Fc-Fc) is typically found around 0.35 V, and a smaller value is generally observed when a chemical spacer is inserted between the two ferrocenyl moieties because of the diminishment of direct metal-metal overlap.<sup>35–37</sup>

(32) Ribou, A. C.; Launay, J. P.; Sachtleben, M. L.; Li, H.; Spangler, C. W. *Inorg. Chem.* **1996**, *35*, 3735–3740.

(33) Levanda, C.; Bechgaard, K.; Cowan, D. O. *J. Org. Chem.* **1976**, *41*, 2700–2704.

(34) Reimers, J. R.; Cai, Z. L.; Hush, N. S. *Chem. Phys.* **2005**, *319*, 39–51.

(35) Brown, G. M.; Meyer, T. J.; Cowan, D. O.; Levanda, C.; Kaufman, F.; Roling, P. V.; Rausch, M. D. *Inorg. Chem.* **1975**, *14*, 506–511.

(36) Levanda, C.; Cowan, D. O.; Bechgaard, K. *J. Am. Chem. Soc.* **1975**, *97*, 1980–1981.

The results are drastically different when the ferrocenyl groups are bound to the particle core through a saturated aliphatic spacer. This is demonstrated experimentally with the Ru=CH-CH<sub>2</sub>-Fc particles (yellow-black dashed curve, Figure 2). Here only one pair of voltammetric waves can be seen with a formal potential of +0.026 V, very similar to that of the ferrocene monomers (Table 1). This suggests that the intervalence transfer is effectively impeded because of the sp<sup>3</sup> carbon spacer, in accord with previous studies of biferrrocene derivatives linked by an ethylene spacer (-CH<sub>2</sub>-CH<sub>2</sub>-)<sup>37,38</sup> and metal nanoparticles functionalized with terminal ferrocene moieties through a saturated linker and/or Au-S bond.<sup>39-42</sup> In these studies, the voltammetric features were found to be consistent with those of monomers of the ferrocene derivatives, indicating little electronic interactions between the ferrocene metal centers.

It is unlikely that the appearance of two instead of one pair of voltammetric peaks as observed above arose from electrostatic interactions between the ferrocene moieties upon electro-oxidation. Such effects have been observed in two-dimensional (2D) self-assembled monolayers of  $\omega$ -ferrocenyl alkanethiols on a gold surface.<sup>43,44</sup> However, the potential splitting ( $\Delta E^{\circ}$ ) is typically less than 100 mV, much smaller than what we observed here with the Ru=CH-Fc particles (Figure 2 and Table 1). Furthermore, the control experiment with the Ru=CH-CH<sub>2</sub>-Fc nanoparticles (Figure 2) strongly discounts this electrostatic hypothesis. This is because of the similar packing and proximity of the ferrocene groups on the Ru=CH-Fc and Ru=CH-CH<sub>2</sub>-Fc particle surfaces. Additionally, one would anticipate a much stronger electrostatic interaction between the ferrocene groups in Murray's fully ferrocenated gold particles<sup>42</sup> and in structurally analogous ferrocenyl-terminated poly(propyleneimine) dendrimers,<sup>45,46</sup> and yet in these systems only a single pair of voltammetric waves was observed. Thus, taken together these results suggest that intraparticle intervalence transfer indeed occurs in the Ru=CH-Fc particles, most probably as a consequence of the  $\pi$  bonding linkage that binds the redox-active ferrocene moiety onto the particle core surface with negligible electrostatic contributions. In other words, direct metal-metal overlap is minimal compared to the through-(ligand)-bond contributions, which is further supported in theoretical modeling and calculations (vide infra).

Two additional experiments were carried out to eliminate the possibility that the appearance of two pairs of voltammetric peaks arose from particle adsorption onto the electrode surface since in solid films the ferrocene moieties might exhibit different

energetic states and accessibility to counterions because of spatial effects. First, the cathodic and anodic current density of the redox peaks was found to be linearly proportional to the square root of potential scan rates, suggesting that the charge-transfer processes were under diffusion control. Second, after the electrochemical measurements in the Ru=CH-Fc particle solution, the Au electrode was taken out and rinsed with copious amounts of DMF and then immersed into a same electrolyte solution without the nanoparticles. Only featureless voltammetric responses were observed, as shown in Figure 2 (blue curve). In short, both measurements signified minimal surface adsorption of the particles.

Furthermore, voltammetric measurements of the organic extract after cyanide dissolution of the Ru=CH-Fc nanoparticle cores exhibited only one pair of peaks (Figure S2). This suggests that the appearance of two pairs of voltammetric waves for the Ru=CH-Fc nanoparticle as shown in Figure 2 is highly unlikely to arise from formation of polyvinylferrocene derivatives that have been found to show splitting of the voltammetric features.<sup>47</sup> This is in good agreement with the mass spectroscopic measurements (Figure S1).

**NIR Spectroscopy.** The notion that intervalence charge transfer occurred within the Ru=CH-Fc nanoparticles was further supported by near-infrared (NIR) spectroscopy using nitrosonium hexafluorophosphate (NOPF<sub>6</sub>) as the oxidizing reagent. Figure 3A shows the NIR absorption spectra of Ru=CH-Fc (sample III) particles with addition of varied amounts of freshly prepared 1 mM NOPF<sub>6</sub> in DMF. A moderately intense absorption peak can be seen at ca. 1930 nm, and the peak intensity exhibits a volcano-shaped dependence on the amount of NOPF<sub>6</sub> added (inset). Again, similar responses were observed for other Ru=CH-Fc particles in the series with different ferrocene surface coverage.

Such a spectroscopic signature is generally taken as a strong indicator that intervalence charge transfer occurs between the ferrocene groups at mixed valence. Importantly, it has been shown previously that the intervalence transfer can exclusively take place through the ligand (bond) system,<sup>32,33</sup> where the spatial separation between the two iron centers is too large to have a meaningful direct overlap. Thus, it is most probable that the intervalence transfer in the Ru=CH-Fc particles also occurs through the ligand bridges because of the Ru-carbene  $\pi$  bonds and the conductive particle core. This is further confirmed in quantum calculations (vide infra).

Table 2 lists the amount of NOPF<sub>6</sub> needed to reach maximum NIR absorption in solutions of the six Ru=CH-Fc particles. Whereas the maximum NIR absorption corresponds to the mixed valence of the ferrocene moieties on the nanoparticle surface (i.e., 50% oxidized to ferrocenium and the remaining 50% at neutral state), it can be seen from Table 2 that the amount of NOPF<sub>6</sub> added at maximum NIR absorption is typically greater than 50% of the ferrocene in the sample (although  $V_{\text{NOPF}_6, \text{max}}$  does increase almost linearly with the amount of ferrocene in the solution), and the deviation increases with increasing ferrocene coverage on the nanoparticle surface. This may, at least in part, be attributable to the capacitive nature of the nanoparticle molecules,<sup>6</sup> where the particle molecular capacitance is anticipated to increase with increasing coverage of the ferrocene moieties on the particle surface. In other words, in addition to oxidation of ferrocene to ferrocenium, addition of the oxidizing reagent (NOPF<sub>6</sub>) will also lead to charging of the

(37) Kadish, K. M.; Xu, Q. Y.; Barbe, J. M. *Inorg. Chem.* **1987**, *26*, 2565-2566.

(38) Morrison, W. H.; Krogsrud, S.; Hendrick, D. N. *Inorg. Chem.* **1973**, *12*, 1998-2004.

(39) Yamada, M.; Quiros, I.; Mizutani, J.; Kubo, K.; Nishihara, H. *Phys. Chem. Chem. Phys.* **2001**, *3*, 3377-3381.

(40) Horikoshi, T.; Itoh, M.; Kurihara, M.; Kubo, K.; Nishihara, H. *J. Electroanal. Chem.* **1999**, *473*, 113-116.

(41) Li, D.; Zhang, Y. J.; Jiang, J. G.; Li, J. H. *J. Colloid Interface Sci.* **2003**, *264*, 109-113.

(42) Wolfe, R. L.; Balasubramanian, R.; Tracy, J. B.; Murray, R. W. *Langmuir* **2007**, *23*, 2247-2254.

(43) Chidsey, C. E. D.; Bertozzi, C. R.; Putvinski, T. M.; Mujisce, A. M. *J. Am. Chem. Soc.* **1990**, *112*, 4301-4306.

(44) Uosaki, K.; Sato, Y.; Kita, H. *Langmuir* **1991**, *7*, 1510-1514.

(45) Cuadrado, I.; Moran, M.; Casado, C. M.; Alonso, B.; Lobete, F.; Garcia, B.; Ibisate, M.; Losada, J. *Organometallics* **1996**, *15*, 5278-5280.

(46) Zamora, M.; Herrero, S.; Losada, J.; Cuadrado, I.; Casado, C. M.; Alonso, B. *Organometallics* **2007**, *26*, 2688-2693.

(47) Pearce, P. J.; Bard, A. J. *J. Electroanal. Chem.* **1980**, *112*, 97-115.

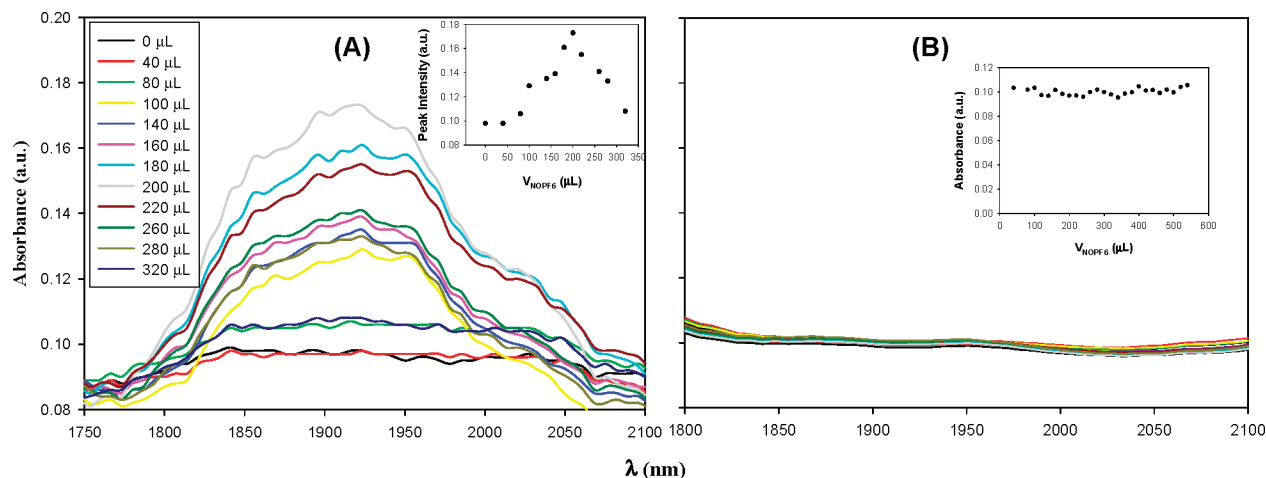


**Figure 3.** NIR spectra of (A) Ru=CH-Fc (sample III) and (B) Ru=CH-CH<sub>2</sub>-Fc nanoparticles with addition of varied amounts of 1 mM NOPF<sub>6</sub>. (A) Amount of NOPF<sub>6</sub> added is shown in the figure legend. (B) Amount was varied from 40 to 540 μL at an increment of 20 μL. Particle concentrations were 0.5 mg in 3 mL of DMF. Insets show the variation of the absorbance at 1930 nm with the amount of NOPF<sub>6</sub> added.

**Table 2.** Variation of the Amount ( $V_{\text{NOPF}_6, \text{max}}$ ) of NOPF<sub>6</sub> (1 mM) Added at Maximum NIR Absorption with the Ferrocene Surface Coverage on the Particle Surface

particles <sup>a</sup>	Fc %	$V_{\text{NOPF}_6, \text{max}}$ (μL)	amount of ferrocene <sup>b</sup> (μmol)
Ru=CH-Fc (I)	5.9	60	0.127
Ru=CH-Fc (II)	6.2	85	0.133
Ru=CH-Fc (III)	10.5	200	0.228
Ru=CH-Fc (IV)	12.9	280	0.277
Ru=CH-Fc (V)	13.5	300	0.290
Ru=CH-Fc (VI)	21.3	300	0.456

<sup>a</sup> The experimental conditions were all the same as those denoted in Figure 3. <sup>b</sup> Estimated by assuming a particle composition of Ru<sub>367</sub>L<sub>71</sub>, where L denotes the surface protecting ligands.<sup>1</sup>

nanoparticle double-layer capacitance (such charging effects may also account for the unequal voltammetric peak currents as shown in Figure 2).<sup>48</sup>

In sharp contrast, when the ferrocene groups are linked by sp<sup>3</sup> carbons to the particle surface no intervalence transfer is anticipated, and consequently, no transition is observed in the NIR region. Experimentally, we observed only a featureless NIR response with the Ru=CH-CH<sub>2</sub>-Fc particles (again by using NOPF<sub>6</sub> as the oxidizing reagent, Figure 3B), and the absorbance remained virtually invariant with addition of NOPF<sub>6</sub> (inset), in good agreement with the voltammetric results (Figure 2).

**Theoretical Simulations and Modeling.** To facilitate a deeper understanding of the fundamental mechanism for the intraparticle charge delocalization, DFT calculations, with hybrid B3LYP functional, were performed for a series of ruthenium cluster models capped with two ferrocene moieties via Ru=C π bonds. Figure 4A shows the highest occupied molecular orbitals (HOMOs) for the model system consisting of a cluster of 17 Ru atoms with two Fc-CH= groups at +1 net charge. The frontier orbitals (HOMOs and LUMOs) can be found to be delocalized Ru metal states. As evidenced in the energy diagram (panel B), the MOs energetically close to the HOMOs/LUMOs are dominated by the band states of the bridging Ru metal cluster.

This is typical for resonance electron transfer (ET) through metals (conductor) where electrons (or holes) go through

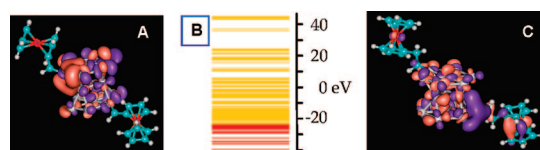


**Figure 4.** (A) HOMO topology and (B) energy diagram of the Ru<sub>17</sub>[=CH-Fc]<sub>2</sub> cluster at the +1 charge state, and (C) the HOMO topology of the Ru<sub>17</sub>[=CH-CH<sub>2</sub>-Fc]<sub>2</sub> cluster at the +1 charge state.

delocalized metal states. In other words, the states in the Ru cluster form an effective conducting medium for the intervalence transfer between different ferrocenyl groups. A positive charge (hole) is first transferred from the Fe(III) center to an occupied Ru band state and then reaches the Fe(II) center of the other ferrocenyl group. Electron transfer is along the opposite direction. These results suggest that the through-bond contributions play a predominant role in nanoparticle-mediated intervalence transfer, consistent with the experimental data (vide ante). In contrast, in the insulator/semiconductor bridge-assisted superexchange ET, the electrons tunnel through “virtual” states.<sup>49</sup> This is demonstrated in Figure S3 with Fc(CH=CH)<sub>3</sub>Fc monocation, where the HOMO is delocalized over the entire molecule. Similar behaviors are observed in monocations of other diferrocenylpolyene derivatives, Fc(CH=CH)<sub>n</sub>Fc.

To have a more quantitative comparison to the experimental data we will need to go beyond the standard DFT study. This is because of the self-interaction errors in most of the current DFT functionals,<sup>50,51</sup> i.e., when the adiabatic state is a mixture of the diabats, the DFT energy is often too low and results in exaggeration of the electron delocalization. Thus, we have opted to employ the constrained DFT (CDFT) method developed by Wu and Van Voorhis.<sup>52</sup> In this method, charge-localized diabatic states (donor and acceptor) are explicitly constructed in the modified DFT calculations, which were performed with a patched version of NWChem<sup>28</sup> using the same basis functions as in the above standard DFT study. First, with respect to Fc-CH=CH-Fc monocation, the relative electronic coupling

(49) van Herrikhuyzen, J.; Portale, G.; Gielen, J. C.; Christianen, P. C. M.; Sommerdijk, N. A. J. M.; Meskers, S. C. J.; Schenning, A. P. H. J. *Chem. Commun.* **2008**, 697–699.

(50) Perdew, J. P.; Levy, M. *Phys. Rev. B* **1997**, *56*, 16021–16028.

(51) Zhang, Y. K.; Yang, W. T. *J. Chem. Phys.* **1998**, *109*, 2604–2608.

(52) Wu, Q.; Van Voorhis, T. *J. Chem. Phys.* **2006**, *125*, 164105.

(48) Pietron, J. J.; Hicks, J. F.; Murray, R. W. *J. Am. Chem. Soc.* **1999**, *121*, 5565–5570.

is estimated to be 1.4 for  $\text{Ru}_{17}[\text{=CH-Fc}]_2$  monocation (Figure 4A), suggesting that the  $\text{Ru}=\text{CH-Fc}$  particle core indeed provides an environment equivalent to the conjugated spacer in  $\text{Fc-CH=CH-Fc}$ . Furthermore, unlike in the diferrocenylpolyene system where the electronic coupling follows the exponential decay law, the coupling in the  $\text{Fc-CH}=\text{(Ru)}_n\text{=CH-Fc}$  system changes much more slowly with respect to the distance variation (e.g., by particle diameter). This finding is consistent with the fact that the Ru nanoparticle is a conductor, which is different from the insulator/semiconductor behavior of the conjugated  $(\text{CH}=\text{CH})_n$  group in diferrocenylpolyenes.<sup>53</sup> To further verify that the electronic communication is actually through the Ru particles (through-bond interaction), we performed calculations where all but the two binding Ru atoms are removed. Zero electronic coupling is observed between the two Fc moieties, indicating that through-space interaction is negligible. Again, this is consistent with the experimental observations (additional computational data are included in the Supporting Information).

We also investigated the effects of chemical spacers on intraparticle charge delocalization by examining the HOMO topology of monocations of  $\text{Ru}_{17}[\text{=CH-X-Fc}]_2$  particle models. For saturated alkyl spacers, e.g.,  $\text{X} = (\text{CH}_2)_n$ , charge delocalization is significantly impeded at mixed valence (Figure S4), akin to those observed above with the  $\text{Ru}=\text{CH-CH}_2\text{-Fc}$  particles (Figure 4C). In contrast, with conjugated spacers such as  $-\text{CH}=\text{CH}-$  and  $-\text{C}\equiv\text{C-CH}=\text{CH}-$ , the HOMOs for the monocations of the corresponding particle models exhibit delocalization characteristics over the Ru particle core (Figure S5), similar to that shown in Figure 4A.

It should be pointed out that there are several limitations of the theoretical treatment. First, because of the computational expenses, only 17 ruthenium atoms were used to model the nanoparticle. Although qualitative conclusions can be drawn from such a model, it would be desirable to develop new computational schemes with more metal atoms included in future study to obtain more accurate results. Second, the solvent

effect has been neglected in our study of the  $\text{Fc-CH}=\text{(Ru)}_n\text{=CH-Fc}$  system. Test calculations have shown that the values of nonadiabatic electronic coupling change upon inclusion of the solvent environment, although the corresponding relative values between the  $\text{Ru}_{17}[\text{=CH-Fc}]_2$  and  $\text{Fc-CH=CH-Fc}$  monocations are not as sensitive. Third, being a single particle theory, DFT or CDFT does not fully account for the correlation effect. Combined with the fact that moderate size basis functions were used in the study, some inherent inaccuracies are anticipated of the values that we obtained. Despite all these limitations, careful calibration calculations on other similar model systems indicate that the qualitative conclusions drawn from our theoretical investigations are reliable (Supporting Information). That is, the ruthenium nanoparticles provide an effective means for electronic communication between particle-bound ferrocenyl functional groups.

## Conclusion

From the above analyses it can be seen that effective electronic communication may occur between the metal centers through the band states of the Ru metal core when a conjugated spacer is used to link the ferrocene moieties onto the particle surface, whereas saturated linkers diminish drastically the intervalence transfer at mixed valence. Additionally, the nanoparticle-mediated intervalence transfer appears to be primarily dominated by through-bond contributions rather than the direct overlap between the metal centers. Effects of the nanoparticle-mediated charge delocalization on relevant optoelectronic properties are currently being examined, and results will be reported in due course.

**Acknowledgment.** This work was supported by grants from the National Science Foundation (S.W.C., CHE-0456130 and CHE-0718190; H.B.W., CHE-0348956). The work also used resources of the National Energy Research Scientific Computing Center, which is supported by the Office of Science of the U.S. Department of Energy under Contract No. DE-AC02-05CH11231. S.W.C. and J.P.K. thank J. R. Davies for synthesis of the octyldiazoacetate compound. F.Z.D. and H.B.W. thank Q. Wu and T. Van Voorhis for assistance in performing the constrained DFT calculations.

**Supporting Information Available:** Complete references 23 and 28, mass spectrometric and voltammetric results of the organic extract after cyanide dissolution of the ruthenium nanoparticle cores, additional computational data, and HOMO topological diagrams of biferrocene derivatives with different chemical spacers and ruthenium clusters functionalized with these functional ligands. This material is available free of charge via the Internet at <http://pubs.acs.org>.

JA803887B

(53) The term superexchange usually refers to bridge-mediated ET in which the intermediate states provide an effective increase in the donor-acceptor nonadiabatic electronic coupling (or termed transfer integral) rather than actual populated sites for stepwise electron hopping. Within this picture, the unoccupied bridge states are higher in energy than that of the donor/acceptor for electron transfer or the occupied bridge states are lower in energy than that of the donor/acceptor for hole transfer. The characteristic of superexchange ET through semiconductors/insulators is the drastic decay of ET rates over the distance that the electron travels, i.e., the effective electronic coupling or conductance decays exponentially versus the ET distance. It should also be mentioned that in the superexchange mechanism the donor-acceptor coupling is usually a combination of through-bond (nearest-neighbor tunneling) and through-space (long distance) interactions. For more detailed discussion, see: Ratner, M. A. *J. Phys. Chem.* **1990**, *94*, 4877-4883.